AIP Journal of Applied Physics

Residual strain gradients in a fully stabilized zirconia sample

Bing Hwang, C. R. Houska, G. E. Ice, and A. Habenschuss

Citation: Journal of Applied Physics **63**, 5351 (1988); doi: 10.1063/1.340351
View online: http://dx.doi.org/10.1063/1.340351
View Table of Contents: http://scitation.aip.org/content/aip/journal/jap/63/11?ver=pdfcov
Published by the AIP Publishing

Residual strain gradients in a fully stabilized zirconia sample

Bing Hwang and C. R. Houska
Department of Materials Engineering, Virginia Polytechnic Institute and State University, Blacksburg, Virginia 24061

G. E. Ice and A. Habenschuss
Oak Ridge National Laboratory Beamline-X14, National Synchrotron Light Source, Brookhaven National Laboratory, Upton, New York 11973

(Received 21 October 1987; accepted for publication 28 January 1988)

Polished and severely ground fully stabilized zirconia samples are examined using primarily x-ray diffraction (XRD). The XRD (111) profile reflections from both samples were broadened asymmetrically compared to that of an annealed sample. The asymmetry results from a *d*-spacing gradient extending from the free surface into undisturbed bulk material. There are two possible origins of this depth gradient, i.e., variations in residual strain or chemical composition. The latter is eliminated by means of x-ray photoelectron spectroscopy which did not reveal a chemical gradient. *d*-spacing profiles for both samples are obtained nondestructively using a trial and error fitting procedure. A maximum compressive strain of $\sim 4\%$ is obtained at the surface of the ground sample which decreases gradually to zero at greater depths. The overall zone is ~ 1–$2\ \mu$m. A similar but smaller compressive zone is found in the polished sample which is followed by a zone of tension. The maximum compressive strain at the surface is $\sim 5\%$ and the overall zone of residual strain is $\sim 0.1\ \mu$m.

I. INTRODUCTION

The use of x-ray diffraction (XRD) to measure a residual strain profile normally requires a systematical removal of thin layers from the surface. This is a destructive process that requires tedious elastic corrections. In this work, we describe a nondestructive *in situ* measurement of the strain profile which requires only one intensity profile. The profile appears as an intensity band and results from a gradient of *d* spacings. We have used this approach for diffusion studies with materials having a range of solubility and an associated variation in lattice parameter.[1] A computer program[2] developed previously for diffusion studies was modified so as to include asymmetrical diffraction optics and surface roughness. The resultant strain profile is calculated from the *d*-spacing profile which is obtained from trial and error fitting of the measured intensity band.

II. XPS STUDY

The fully stabilized zirconia (FSZ) samples examined in this work contain 8 mol % Y_2O_3 as a stabilizer. These samples are completely cubic with some Y atoms replacing Zr atoms to form a solid solution. Vacancies are created in the oxygen sites to maintain electrical neutrality. Because Y^{+3} ions have much larger sizes than Zr^{+4} ions (1.051 Å vs 0.84 Å in radii), a composition gradient of Y^{+3} could produce a lattice parameter gradient and a related peak broadening. XPS work was carried out to examine this possibility.

X-ray photoelectron spectroscopy (XPS) scans from both the polished and the severely ground samples showed the presence of O, Zr, Y, Al, and C atoms at the free surface of both samples. Ion milling with Ar^+ ions, together with Mg$K\alpha$ radiation, were used to examine the concentrations of these atoms at various depths below the surface. The concentration of each element is shown as a function of cumulative milling time in Fig. 1 for the polished and ground samples. Carbon deposition on the sample surface was quickly milled away and represented normal contamination from the vacuum system. As the concentration of surface carbon drops, the concentrations of other elements rise quickly and reach constant values within a couple of minutes. This indicates that the samples are homogeneous except in a very small surface region contaminated by carbon. Both polished and ground samples give very similar depth profiles and do not show the large differences found by XRD. We conclude that the measured *d*-spacing gradients cannot be related to a chemical gradient.

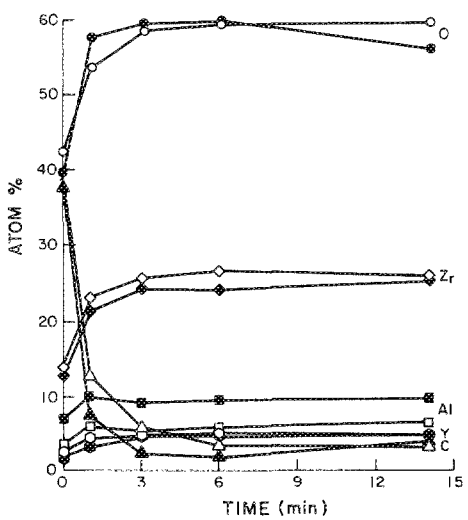

FIG. 1. XPS depth profiles of atomic concentrations for polished and ground FSZ samples. Polished: ●, oxygen; ◆, zirconium; ■, aluminum; ○, yttrium; ▲, carbon. Ground: ○, oxygen; ◇, zirconium; □, aluminum; ○, yttrium; △, carbon. Yttrium points coincide.

 0021-8979/88/115351-06$02.40

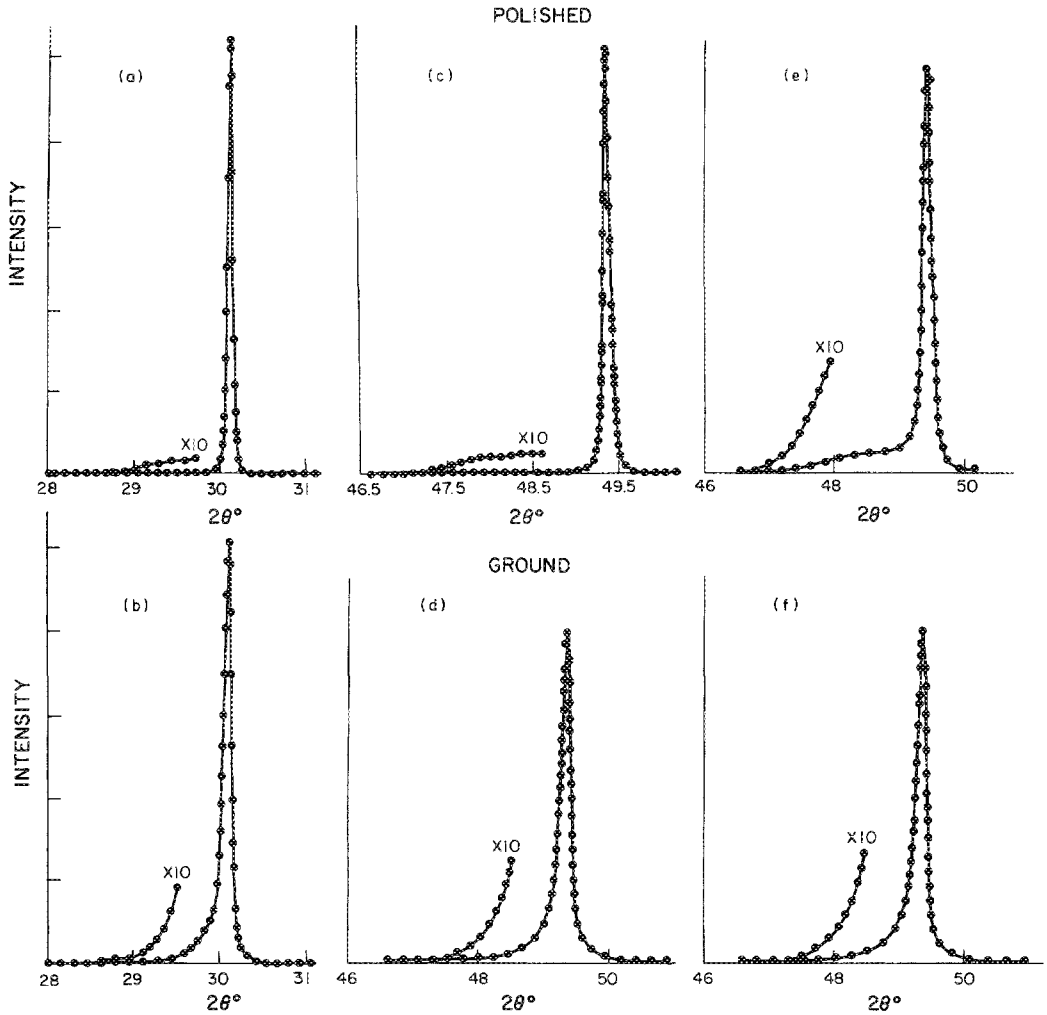

FIG. 2. (111) intensity bands from polished and ground samples showing experimental data points and computer simulations (solid lines) for (a) and (b) symmetrical optics with Cu$K\alpha_1$ radiation ($\lambda = 1.5406$ Å), (c) and (d) synchrotron radiation with $\lambda = 2.4797$ Å and (e) and (f) 3° asymmetric optics with $\lambda = 2.4797$ Å.

III. RESIDUAL STRAIN STUDY BY XRD

A. Measurements of the (111) profiles of the FSZ samples

The (111) peak profiles of the polished and the ground FSZ samples were obtained by point counting using Cu$K\alpha_1$ radiation and symmetrical diffraction optics. Counting at each point was stopped at either 8000 counts or 1000 s, whichever was reached first. The Cu$K\alpha_1$ component was obtained using a diffracted beam quartz monochromator and a fine focus Cu tube. Results from the polished and ground samples are shown in Figs. 2(a) and 2(b). Both profiles extend asymmetrically toward the low-angle side. The ground sample also shows a peak shift relative to that of the polished sample.

The (111) profiles of the polished and the ground samples were also measured using synchrotron radiation of 2.4797 Å with symmetrical and asymmetrical optics at the Oak Ridge National Laboratory beamline (National Synchrotron Light Source) before annealing. The profiles measured with symmetric diffraction optics are shown in Figs. 2(c) and 2(d), respectively, for the polished and the ground samples. Again intensity bands are observed in the profiles of the ground and polished samples. To emphasize the near-surface region, (111) profiles of both samples were measured with asymmetrical diffraction optics [Figs. 2(e) and 2(f)]. Asymmetric diffraction optics were obtained by tilting the sample normal toward the diffracted beam by an amount such that the incident angle is 3°. The small incident angle results in shallower penetration, and as expected influences the peak profile for the polished sample. The peak profile of the polished sample obtained with asymmetrical diffraction optics enhances the low-angle side compared to that found with the symmetrical optics. For the ground sample, no change was observed between the profiles obtained with symmetrical and asymmetrical optics. This unexpected result will be discussed later.

After both samples were subsequently annealed at 1200 °C for 1 h and furnace cooled, the profiles were indistinguishable (Fig. 3). Considerable sharpening was observed. In order to double check our findings, the polished and annealed samples were repolished using alumina powder. No peak shift was observed and the profile was asymmetric toward the low-angle side. This reconfirms the conclusion that the polishing process introduces a low-level intensity band

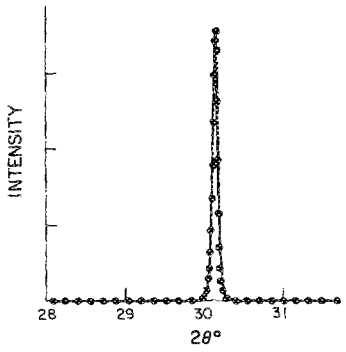

FIG. 3. (111) peak profile of annealed samples (symmetric optics, Cu$K\alpha_1$). ●, experimental data; solid line, Pearson-VII function.

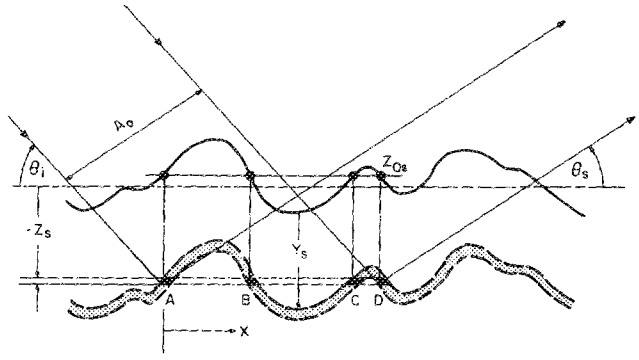

FIG. 4. Schematic diagram showing layer of constant d spacing in rough sample.

and remains unshifted at the main peak. The peak shift between the profiles of the ground and polished samples before annealing is real and due to the extended range of the strain gradient in the severely ground sample. This will be discussed later.

B. Fitting of the experimental intensity bands

The profile of the annealed sample shown in Fig. 3 is fitted with a Pearson-VII function,[3]

$$Y = Iy_0\{1 + [(2\theta - 2\theta_0)^2/ma^2]\}^{-m}, \quad (1)$$

where I and $2\theta_0$ determine the intensity and the peak position while a and m describe the peak width and shape. y_0 is a normalization factor given by

$$y_0 = (1/a\sqrt{\pi m})\{\Gamma(m)/[\Gamma(m-\tfrac{1}{2})]\} \quad (2)$$

with

$$\Gamma(m) = \int_0^\infty x^{m-1}e^{-x}dx \quad \text{and} \quad m > 0.$$

The full width at half-maximum (FWHM) is

$$W = 2a[m(2^{1/m} - 1)]^{1/2}, \quad (3)$$

when $m = 1$, 2, and ∞ the Pearson-VII function becomes a Cauchy, modified Lorentzian, and a Gaussian function, respectively. A value of $m = 20$ is sufficient to represent a Gaussian shape. The Pearson-VII fit for the annealed peak is shown in Fig. 3 as the solid line. Fitted a and m values are 0.032° and 1.8, respectively. Because the annealed sample is strain-free, these a and m values are characteristic of the instrumental broadening and should represent the minimum broadening for the ground and polished samples.

Profile asymmetry was fitted with the d-spacing profiles by using a trial and error procedure. With depth measured from a local surface asperity, the sample can be treated as a system of thin curved layers located at various depths (Fig. 4). The d spacing of each layer is treated as a constant and the corresponding intensity is calculated using a generalized theory presented in the Appendix. The polished sample is flat with the layers parallel to the sample surface, while the ground sample is rough and the layers follow the same fluctuation as the surface profile. The generalized theory treats the intensity from each layer considering the absorption factor for both the flat and the rough samples under both the symmetrical and asymmetrical diffraction optics. Because the d spacing changes continuously from one layer to another, the intensities are spread over a 2θ range according to Bragg's law. In order to fit the intensity data, one must sum Pearson-VII functions. The computer-simulated intensity band is then compared with the experimental data and the d-spacing profile is adjusted accordingly until the simulation and the experimental data show agreement. The results of these fittings are shown in Figs. 2(a)–2(f) as the solid lines. Both the measured and simulated profiles are expanded vertically by ten times at the low-angle side to better show the final fit. d-spacing profiles have been expressed by the following analytical forms:

$$d = d_0 + \sum_{i=1}^{4} \Delta d_i e^{-Y_s/d_i}, \quad (4a)$$

$$d = d_0 + \sum_{i=1}^{4} \Delta d_i \operatorname{erf} c^{-Y_s/d_i}. \quad (4b)$$

For the polished sample, a Gaussian term of the form

$$\Delta d_i \exp[-(Y_s - Y_0)^2/d_i] \quad (4c)$$

was required to put a small hook in the strain profile very close to the surface. These forms should be treated as convenient for fitting experimental intensity bands, and no theoretical significance should be attached to them. Strain profiles are obtained from the d-spacing profiles using $\epsilon = (d - d_0)/d_0$, where d_0 is the asymptotic d-spacing value in the unstrained bulk material. Strain profiles obtained from Eqs. (4a)–(4c) are plotted in Figs. 5 and 6.

IV. DISCUSSION

Separate determinations of the average strain profiles for the polished sample obtained under widely different

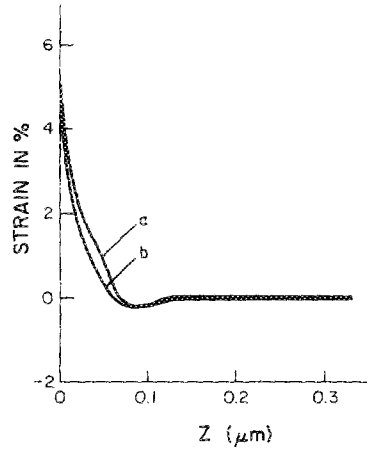

FIG. 5. Depth profiles of strain for polished sample obtained under the following conditions: (a) symmetrical optics using Cu$K\alpha_1$ ($\lambda = 1.5406$ Å) and $\lambda = 2.4797$ Å (synchrotron radiation); (b) asymmetric optics with $\lambda = 2.4797$ Å (synchrotron radiation).

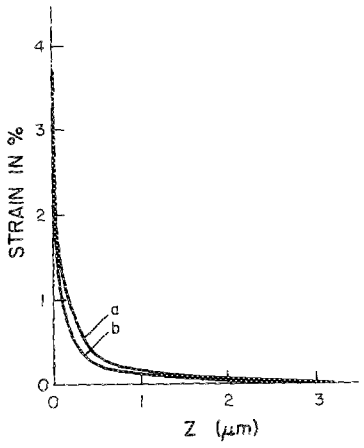

FIG. 6. Depth profiles of strain for ground sample obtained with symmetrical optics. (a) Cu$K\alpha_1$ radiation, (b) $\lambda = 2.4797$ Å (synchrotron radiation).

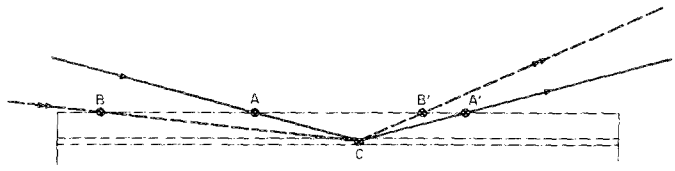

FIG. 7. Absorption path lengths of the symmetric and asymmetric optics for a flat sample.

beam absorption conditions are shown by curves (a) and (b) of Fig. 5. The differences result from changes in instrumental conditions and therefore represent the uncertainty of the method. A change in radiation from $\lambda = 1.5406$ to 2.4797 Å did not produce a measurable difference in curve (a) although the beam penetration for Cu$K\alpha_1$ is twice that for the longer wavelength. Asymmetric optics gave curve (b). The same agreement between results from different measurements made on the ground sample is seen by curves (a) and (b) of Fig. 6. Table I summarizes these findings and includes penetration distances causing the incident and scattered beam to be decreased by e^{-1}. These vary from about 2 to 0.2 μm depending upon the preceding conditions.

Results from the polished sample show a large compressive strain at the sample surface, which decreases rapidly at greater depths. The near-surface compressive zone is followed by a relatively small zone of tension before the strain-free bulk region is reached. The overall strained zone is limited to about 0.1 μm. Strain profiles for the ground sample show a much larger compressive zone extending to about 1–2 μm. No zone of tension is observed probably because the measurements are not sensitive to a small amount of tension located well below the surface. Although the maximum strain of 5% at the polished surface appears to be large, it is compatible with a result found in wear debris.[4] It is interesting to find that the maximum strain at the ground surface is only ~4%. A possible explanation is the top layer of the ground sample had probably reached the same high strain of 5%, but fractured as debris leaving a lower strain in the surface. This is reasonable if one looks at differences between grinding and polishing processes.

Figures 5 and 6 illustrate curves that decrease in a simple way giving strains that vanish at depths of several tenths to several microns depending upon the surface treatment. There are no results suggesting that the strain profiles resulting from surface deformation should be more complex with additional maxima and minima. If this were the case, the x-ray technique must be combined with a suitable mechanical model. And, the fitting procedure should be carried out in a way that is consistent with both the observed intensity and the model (see Ref. 5). When high spacing gradients are observed that are nearly uniform over the lateral dimensions of a sample, oscillations may appear in the diffraction pattern.[6] These were not observed probably because small fluctuations along the lateral directions caused them to cancel out.

As expected, the intensity in the low-angle portion of the peak profile of the polished sample is enhanced when the diffraction optics changes from the symmetrical to asymmetric condition. This absorption enhancement is purely optical and due to the small angle of the incident rays as they impinge upon a flat surface. The corresponding enhancement is not observed for the ground sample. This can be explained qualitatively by the following argument. Consider a horizontal layer located at a depth $|Z|$ below a flat surface (Fig. 7). A signal generating element C belonging to this layer has an absorption length of $AC + CA'$ with symmetrical diffraction optics. The total absorption length is greatly increased to $BC + CB'$ when asymmetric diffraction optics is used. For the present case, the incident angle is changed from ~25° to 3°, which gives an intensity decrease of e^{-1} at depths of 0.9 and 0.2 μm, respectively, for $\lambda = 2.4797$ Å. A similar path change does not occur with the ground sample. The ground sample was roughened to give a σ standard deviation of 6.2 μm for excursion heights measured from the mean surface. The surface may be considered as roughness mountains and valleys. With a small incident angle of 3°, the valleys become somewhat hidden in the shadow of the mountains and contribute little intensity. Therefore, the intensity from the mountain tops becomes weighted heavily in

TABLE I. Results, conditions, and data locations for a FSZ sample deformed by polishing and severe grinding.

FSZ sample	λ (Å) optics	e^{-1} penetration (μm)	Surface roughness σ (μm)	Profiles XRD strain Figs.	Maximum % compressive strain	Near-surface compressive zone size (μm)	Near-surface tension zone size (μm)
Polished	1.5406 symmetric	2.1	0.027	2(a), 5(a)	5.0	0.07	Small (0.07–0.11$^+$)
Polished	2.4797 symmetric	0.9	0.027	2(c), 5(a)	5.0	0.07	Small (0.07–0.11$^+$)
Polished	2.4797 3° symmetric	0.2	0.027	2(e), 5(b)	5.0	0.06	Small (0.06–0.11$^+$)
Ground	1.5406 symmetric	···	6.2	2(b), 6(a)	3.7	2.0	Not observed
Ground	2.4797 symmetric	···	6.2	2(d), 6(a)	3.7	1.5	Not observed
Ground	2.4797 3° symmetric	···	6.2	2(f), 6(b)	3.7	1.5	Not observed

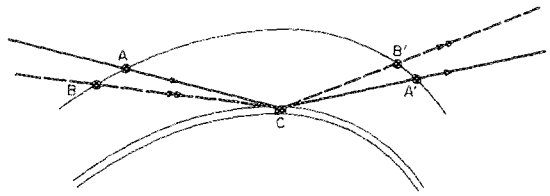

FIG. 8. Absorption path lengths of the symmetric and asymmetric optics for a curved sample.

the averaging process. A layer below the free surface is depicted in Fig. 4. As is seen in Fig. 8, when the surface is curved downward, tilting the sample to give a low incident angle gives nearly the same path lengths. This would result in a smaller reshaping of the intensity bands relative to an ideally flat sample. Although sizeable changes in path lengths are expected at the valleys of a surface, these points are de-emphasized for the present conditions by a shadow effect.

We obtained the same values of a and m using the Pearson-VII function in fitting the full profiles from polished, ground, and annealed samples provided the data are collected with the same x-ray optics. This means that neither polishing nor grinding operations generate sufficient defects to give measurable line broadening. One should not infer from this finding that those particles lost from the surface as debris are like that surface material that remains intact. In fact, it has been found that wear debris collected from a partially stabilized zirconia is highly defective, displaying high levels of nonuniform strain and a small x-ray particle size.[4] Both findings are indicative of a high dislocation density. Highly strained asperities susceptible to fracture represent a small volume fraction of surface material, whereas all debris particles originate from such localized regions. It appears that the averaging taking place in the diffraction process favors the large volume fraction of material having higher crystalline perfection. Also, the large surface to volume ratio for debris particles offers a special quenching mechanism allowing the defect structure to be retained. The thermal environment of residual material remaining in good contact with the surface is very different because of slower cooling rates. The latter would give a less disturbed or an annealed crystalline structure.

ACKNOWLEDGMENTS

This work was made possible by the Energy Conversion and Utilization Technologies Division of the Department of Energy under Contract No. 7733, PAX-09, S/A1. We would like to thank C. Yust of the Oak Ridge National Laboratory for having the samples prepared and for his helpful discussions. Also, we are greatly indebted to Rich Neiser for his technical assistance at the National Synchrotron Light Source. Research was performed in part at the Oak Ridge National Laboratory Beamline X-14 at the National Synchrotron Light Source, Brookhaven National Laboratory, sponsored by the Division of Materials Sciences and Division of Chemical Sciences, U. S. Department of Energy, and under Contract No. DE-AC05-840R21400 with the Martin Marietta Energy Systems, Inc.

APPENDIX

Figure 9 is a schematic diagram showing the ray optics of the x-ray measurement. For a single-phase flat sample without a texture, the diffraction intensity contributed by a small horizontal layer of thickness ΔZ is given by

$$\Delta I = I_0 Q e^{-\mu[|Z|/\sin(\theta+\omega)+|Z|/\sin(\theta-\omega)]}\Delta V, \qquad \text{(A1)}$$

where I_0 = the incident intensity;

$$Q = \text{const} \times \frac{\lambda^3}{v_c^2} \frac{1+\cos^2 2\theta \cos^2(2\theta')}{\sin\theta \sin(2\theta)} jF^2 \qquad \text{(A2)}$$

with λ = wavelength of the incident beam, v_c = volume of the unit cell, 2θ = Bragg angle, $2\theta'$ = Bragg angle for the diffracted-beam monochromator, j = multiplicity, and F = structure factor. The exponential term is the absorption attenuation factor with μ = the linear absorption coefficient, $|z|$ = the depth of the signal generating layer, ω = the tilt angle of the sample normal toward the incident beam from the symmetrical position, $\theta + \omega = \theta_i$ = the incident angle, $\theta - \omega = \theta_s$ = the signal angle, and ΔV = the volume of the small layer $= A_0 \Delta Z / \sin(\theta + \omega)$ with A_0 = the cross-sectional area of the incident beam. The parameters defined above also appear in corresponding expressions for the rough sample.

While the intensity calculation for a flat sample is straightforward, the corresponding calculation for a rough sample is complicated by variations in beam lengths for rays entering and leaving the sample. The diffracted intensity from a rough sample of uniform d spacing was developed in a separate work.[7] This statistical model uses a normal distribution to describe the heights of surface excursions and an exponential function to describe the correlation of the excursion heights along the horizontal direction. We begin with this model and extend it so as to include a d-spacing gradient.

Figure 4 illustrates a rough layer with the following two vertical locations: (1) Z_{0s}, the scaled layer position from the mean plane; (2) Y_s, the scaled depth of the signal element from the free surface. The scaling factor is $\sqrt{2}\sigma$ with σ designating the standard deviation of the height distribution. Z_s ranges from negative to positive values, while Y_s is always positive. A thin curved layer located at a depth Y_s is assumed to have the same d spacing and varies only with Y_s.

Consecutive layers of spacing d_j are at a depth Y_s^j and contribute intensity I_j. The intensity profile from each layer

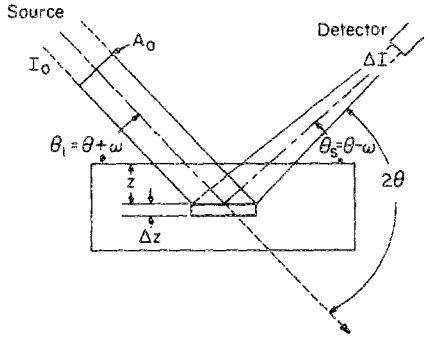

FIG. 9. Diffraction optics illustrating quantities defined in the Appendix.

is described by a Pearson-VII function which accounts for the instrumental and sample broadening. An intensity band is due to all layers and is obtained by summing the individual contributions, i.e.,

$$P_B(2\theta) = \sum_j I_j y_0 \left(1 + \frac{(2\theta - 2\theta_j)^2}{ma^2}\right)^{-m} . \quad \text{(A3)}$$

While the I_j's need to be calculated from the roughness model, a, m, and $2\theta_j$'s can be adjusted by trial and error to the fit of the measured intensity band. The quantities a and m are usually obtained at the extremities of an intensity band. In the present samples a and m are constants while the $2\theta_j$ values are determined from Figs. 4(a)–4(c) and Bragg's law.

The intensity I_j from a general layer at Y_s^j for a rough sample has been treated elsewhere.[7,8] Layer Y_s (see Fig. 4) is divided into like groups. For example, elements A and B belong to the same group at Z_s and depth Y_s^j designated by (Z_s, Y_s^j). The surface excursion corresponding to the elements of group (Z_s, Y_s^j) is located at $Z_{0s} = Z_s + Y_s^j$. In the present model, the incident and signal rays are assumed to intersect the surface profile only once. If the intersecting point is located at a scaled height of Z_{ss}, the corresponding absorption length for the signal ray from (Z_s, Y_s^j) group is

$$l_s = \sqrt{2}\sigma[(Z_{ss} - Z_s)/\sin\theta_s] . \quad \text{(A4)}$$

A similar relation is required for the incident path, i.e., l_i. The average absorption factor for group (Z_s, Y_s^j) involving both paths is defined by

$$A(Z_s, Z_{0s}) \simeq \langle e^{-\mu l_i}\rangle \langle e^{-\mu l_s}\rangle \quad \text{(A5)}$$

with l_i and l_s coupled through the intermediate location of the signal element.

The first and second terms on the right-hand side of Eq. (A5) are the average attenuation factors for the coupled incident and signal rays. $\langle e^{-\mu l_i}\rangle$ is obtained from the function $p(l_i)dl_i$ giving the probability of finding an absorption length in the incident beam between l_i and $l_i + dl_i$:

$$\langle e^{-\mu l_i}\rangle = \int_0^\infty e^{-\mu l_i} p(l_i) dl_i .$$

Writing this in terms of the Z coordinate,[7,8]

$$\langle e^{-\mu l_i}\rangle = \frac{1}{\sqrt{\pi}} \int_{Z_s}^{4} e^{-[\sqrt{2}\sigma\mu(Z_{is} - Z_s)/\sin\theta_i]} \times e^{-[(Z_{is} - \rho Z_{0s})^2/(1-\rho^2)]} \times \left(\frac{1}{\sqrt{1-\rho^2}} - \frac{\rho^2 Z_{is} - \rho Z_{0s}}{\tau_{cs}\tan\theta_i (1-\rho^2)^{3/2}}\right) dZ_{is} . \quad \text{(A6)}$$

The corresponding term $\langle e^{-\mu l_s}\rangle$ is evaluated, by a similar expression.

For the signal generating elements in (Z_s, Y_s^j) group, Z_{is} ranges from Z_s to infinity. The upper limit of Z_s in Eq. (A6) is truncated at 4 because only 0.01% of the surface profile is located above $Z_s = 4$. Each point absorber along either l_i or l_s is related to the surface asperity at the signal element (Z_{0s}) through ρ, the autocorrelation coefficient function,

$$\rho = e^{-\tau_i/\tau_c} . \quad \text{(A7)}$$

It should be clear that the relative distance τ_{ss} or τ_{is} are projections along the x axis (Fig. 4). τ_c is the correlation distance which, along with σ, is obtained from profilometer measurements. Similarly, $\langle e^{-\mu l_s}\rangle$ can be obtained from Eqs. (A6) and (A7) with θ_i and τ_i replaced by θ_s and τ_s.

The intensity from a general layer with thickness Δt_j is[7,8]

$$I_j = I_0 A_0 Q \left(\frac{\sqrt{\pi}}{2} e^{\sigma^2[(\mu/\sin\theta_i) + (\mu/\sin\theta_s)]^2/2 - \sqrt{2}\sigma Y_s^j[(\mu/\sin\theta_i) + (\mu/\sin\theta_s)]} \times \left\{1 + \operatorname{erf}\left[3 + Y_s^j - \sqrt{2}\sigma\left(\frac{\mu}{\sin\theta_i} + \frac{\mu}{\sin\theta_s}\right)/2\right]\right\} + \frac{1}{\sqrt{\pi}\sin\theta_i} \int_{-4}^{+4} A(Z_s, Z_{0s}) e^{-(Z_s + Y_s^j)^2} dZ_s\right) \Delta t_j . \quad \text{(A8)}$$

Z_s extends over the range ± 4. However, for $Z_s < -4$ a flat sample calculation is used. Equation (A8) is integrated numerically and this result is used in Eq. (A3) to construct the intensity band.

[1] C. R. Houska, Treatise Mater. Sci. Technol. **19A**, 63 (1980).
[2] J. Unnam, D. R. Tenney, J. A. Carpenter, and C. R. Houska, College of Engineering, VPI, SU, and NTIS Report No. VPI-E76.9 (1976).
[3] M. M. Hall, V. G. Veeraraghavan, H. Ruben, and P. G. Winchell, J. Appl. Crystallogr. **19**, 66 (1977).
[4] S. Rao and C. R. Houska, Acta Crystallogr. A **42**, 14 (1986).
[5] J. Unnam, J. A. Carpenter, and C. R. Houska, J. Appl. Phys. **44**, 1957 (1973).
[6] S. Rao and C. R. Houska, Acta Crystallogr. Sect. A **41**, 513 (1985).
[7] B. Hwang and C. R. Houska, J. Appl. Phys. **63**, 5346(1988).
[8] B. Hwang, Ph. D. thesis (Virginia Polytechnic Institute and State University, 1987).